行政院原子能委員會

委託研究計畫研究報告

【應用於太陽能轉換之量子點敏化 InN/TiO_2 奈米粒子薄膜研發】

【Quatum-Dot Enhanced InN/TiO_2 Nanoparticle Films for Solar Energy Conversion Applications】

計畫編號：952001 INER 028

受委託機關(構)：國立交通大學

計畫主持人：林明璋

核研所參與人員：

聯絡電話：(03)5731696

E-mail address：chemmcl@emory.edu

報告日期：95 年 12 月 1 日

目　錄

中文摘要

本計畫是為期三年行政院原子能委員會委託研究計畫之第二年執行結果摘要。本年的主要工作在進行以下目標：利用不同大小的半導體量子點(QD)取代有機染料，改善其不穩定的缺點。在半導體量子點敏化的研究中，選用不同的鋪化物及金作為吸收太陽能的敏化物。同時，以 InN 覆蓋量子點與 TiO_2 混合作基板功能的研究也在進行，基板導電的好壞影響太陽能轉換的效率，所以 TiO_2 基板品質的提昇，亦是本年度研究重心之一。

在上述不同角度上的努力，目前太陽能轉換效率已從去年底 nA 左右的光電流增進 30 幾倍，同時，N_3-dye/TiO_2 系統的 AM1.5 光電流偵測已達到 6.8 %的效率。另外，在一系列的量子點-二氧化鈦混合作基板，InN/QD-TiO_2 系統的光電流，亦有大幅增加。目前，最高效率已達到 0.22 %光電效用，未來一年期望效率可高達 3-5 %。

Abstract

With very scarce natural energy resources, Taiwan should invest with high priority in renewal energy research. In this area of scientific endeavor, Taiwan is lagging very far behind Japan, the US and Europe. The Sun is an inexhaustible natural energy source, efficient utilization of solar energy should be one of the most important technological challenges of the 21st century.

In the proposed studies at NCTU, we focus primarily on the development of an economically viable solar energy conversion system for photovoltaic and/or photo-electrochemical water-splitting applications. The low-cost, nontoxic and chemically and thermally stable properties of TiO_2 have resulted in much recent research effort to circumvent its large band gap (3.2 eV or 387 nm) by modifying its surface optical properties for applications in the visible region of the spectrum, specifically for solar energy conversion. The best known technique to enhance its photovoltaic efficiency is Graetzel's method using dyes to improve its photoabsorption cross section and electron transfer dynamics.

The best dye employed by Graetzel and co-workers, $RuL(SCN)_3$, has reached ~10% solar energy conversion efficiency under their best operational conditions. It is comparable to amorphous silicon systems with 9-10% efficiencies and is less than that of polycrystalline silicon devices which have been reported to reach >15% efficiency. It should be noted that both the organic dye/TiO_2 and polycrystalline Si systems are costly and still cannot compete economically with fossil fuels such as oils and natural gases.

In the past year, we have focused on studies of the effects of InN nanoparticle size and of a variety of In-containing semiconductor quantum dots at the interface of InN and TiO_2 on the devices' photocurrents. In addition, we have attempted to improve the quality of the TiO_2 substrate using different sol gel preparation methods as well as mixing TiO_2 with quantum dots of Au, In_2S_3, In_2O_3, among others.

For pure TiO_2 substrates, we have now achieved 6.8% efficiency for the N_3-dye/TiO_2 test device. Overall, we have characterized many samples with AM1.5 simulation and have obtained >0.2% photo-electric conversion efficiency.

壹、計畫緣起與目的

由於天然能源的缺乏，台灣每年約有 98 %的能源仰賴進口。因此，台灣應該優先地投資在再生能源的研究領域。在此科學領域中，台灣已遠遠落後於日本、美國和歐洲。太陽是一個取之不盡、用之不竭的天然資源，因此有效率地使用太陽能應是二十一世紀最重要的科技挑戰之一。

此計畫將在交通大學執行，但和核能所密切合作。我們主要著重於發展一個具經濟效益的太陽能轉換系統以應用在太陽能光電轉換及/或光電化學上分解水的研究。二氧化鈦(TiO_2)的低成本、無毒性、及化學及熱穩定的性質，使得相當多的研究群組致力於研究如何透過表面光學特性的修飾以克服其較大的 band gap（3.2 eV 或 387 nm），以將其應用於可見光區，尤其是太陽能之轉換。而提升其光電效率的最著名的技術乃是 Graetzel's 所發展出以染料改進半導體之光吸收截面積及電子轉移動態學的方法。

Graetzel 等人使用最理想的染料，在最佳的實驗條件下，已可達到 10 %的太陽能轉換效益，其轉換效益和非晶形矽系統的 9-10 %相當，但比多晶形矽系統的>15 %差。值得注意的是，有機染料/TiO_2及多晶形矽系統之成本較高，其經濟效益仍然無法與石化燃料，如石油及天然氣相比。

於是我們希望可以利用半導體量子點取代有機染料，改善其不穩定的缺點。在半導體量子點敏化的研究中，選用矽、磷化銦及其他半導體或導體作為吸收太陽能的敏化物。矽及磷化銦量子點的能隙大約是 1.6ev 左右，可以吸收太陽光中大量的輻射能量(太陽光

中已可見光及紅外光含量最多)。

在 Emory 大學，林明璋研究組已經成功地利用低壓有機金屬化學蒸鍍法（OMCVD），使用 HN_3 及 $In(CH_3)_3$，將所產生的 InN 薄膜沈積在已吸附固定於 sapphire 片或 Ti 金屬上之 TiO_2 奈米粒子上[1]。此沈積的 InN/TiO_2 奈米粒子薄膜呈現非常寬廣的 390-800 nm 紫外/可見光吸收譜帶，其吸收光區與 Graetzel[2] 等人的 black dye/TiO_2 系統所量測的結果相當類似。此半導體的 InN/TiO_2 薄膜其穩定的化學性質或許有助於其利用於光電轉率及水分解應用上的耐用性。在後者的應用上，已有類似的方法使用 InGaP/GaAs 光電極可達到令人印象深刻的 12.4 %轉換效率[3]。相較於 InGaP/GaAs 系統在光電化學之應用上，InN/TiO_2 奈米粒子薄膜其化性較穩定且製造成本更便宜。

InN/TiO_2 奈米薄膜在光電轉換之電子轉移等物理特性將利用交通大學的超快雷射技術來研究，而其光電子產生及轉移的效率則可以利用光電流的直接量測而得到。在台灣，超快雷射技術應用於凝態的研究，交通大學應用化學系居於領先之地位。

除了我們所量測到增強的 InN/TiO_2 薄膜在紫外/可見光區吸收，最近 Nozik 等人已經偵測到以 InP 量子點吸附在 TiO_2 奈米薄膜上，其在紫外/可見光區之吸收有顯著的提升[4,5]。由於物理吸附之作用力通常不強，且 InP 不夠耐用，所以 Nozik 的 InP/TiO_2 系統大概無法長久的使用，尤其在溶液中使用。因此，是否可以利用有機金屬蒸鍍法以一層化性穩定之 InN 薄膜，將這些量子點包覆起來？若可以這麼做，這些以 InN 包覆的 InP 量子點或其他類似的高效率光電轉換材料所產生的光電子是否能有效率地轉移到 TiO_2 上？這些

是我們在發展一個有效率和具經濟效益的光電轉換及水分解系統的過程中，希望能有系統來探討的問題。

在此計畫中，我們擬議研究以 InN 包覆奈米粒子的效應。最初，我們將研究嵌入 Si 及 InP 兩種量子點在 InN 和 TiO_2 奈米薄膜之間，如前所述。Si 和 InP 均具有相似之能隙(分別為 1.1 與 1.3 eV)。除此之外，我們將以其他金屬氧化物之量子點或奈米粒子修飾 TiO_2 基版，以改變 TiO_2 的能帶邊(band edge)，使其與 InN 奈米薄膜或量子點的重疊變為最大。除 Si 及 InP 兩種量子點外，其他各種量子點包含金屬及金屬氧化物，均為研究的對象。

貳、研究方法與過程

一、NH_x（x = 1, 2）自由基之催化產生（王念夏、林明璋）：

。 NH_x(x = 1, 2) Generation via Thermal Decomposition of NH_3 on W and Pt/Rh Alloy

In order to access the possibility of forming InN on TiO_2 substrate via NHx radical reaction with $In(CH_3)_3$, the decomposition of NH_3 on hot W and Pt/Rh surfaces was studied in a laser photolysis/laser induced fluorescence (LP/LIF) system. A Nd/YAG laser-pumped dye laser system (Figure 1a) was used to generate radiations at 336.1 nm and 597.7 nm to monitor NH and NH_2, respectively. NH_3/He (or N_2) mixture was flown into the system through a movable inlet and contacted the hot catalysts at the tip of the inlet. The products were detected ~2 cm downstream. (Figure 1b)

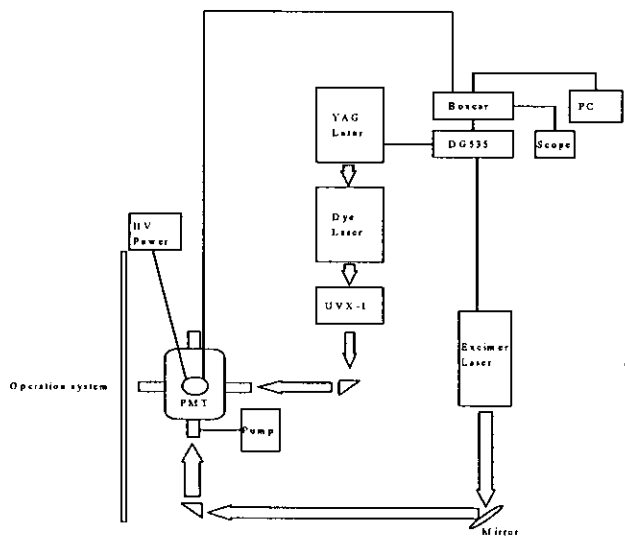

Figure 1a. The LP/LIF system.

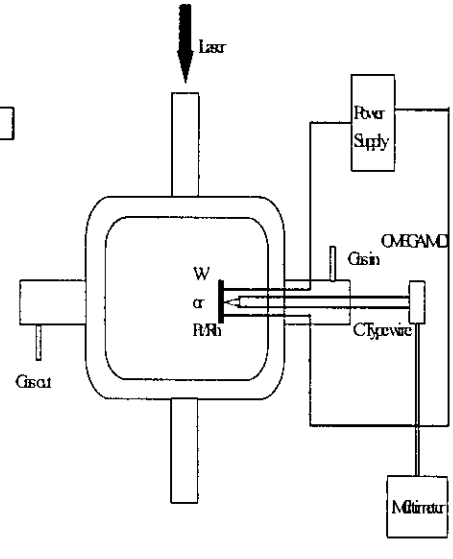

Figure 1b. Reactor used to decompose NH_3.

The concentrations of NH and NH_2 were calibrated via 193 nm photodissociation of HN_3 (for NH) and NH_3 (for NH_2) coupled with the LIF detections.

We have observed NH radicals in both W (T = 1350 – 2100 K) and Pt/Rh (T = 1100–1200 K) systems. Our results showed that Pt/Rh alloy is more efficient than W in decomposing NH_3, as shown in Figure 2.

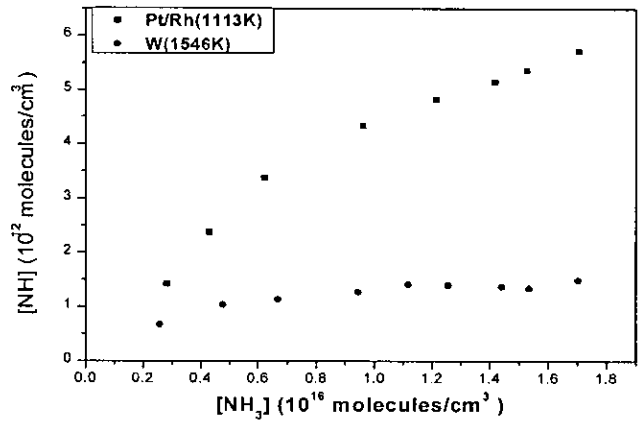

Figure 2. Yield of NH on Pt/Rh at 1113 K and W at 1546 K

This makes Pt/Rh a better choice over W as NH_3 decomposition catalyst.

Efforts have also been made to investigate NH_2 radicals as a product of the decomposition. Our results showed that NH_2 was either not produced on the surfaces, which agreed with an earlier work of Prof. Lin's research group[6], or its concentration was lower than the detection limit, 5 x 10^{12} molecule cm^{-3}. However, a study of NH_3 decomposition on W by Umemoto et al. [7] yielded a different conclusion. They observed both NH and NH_2 in their system and concluded that NH_2 was the primary product but not NH. They attributed the formation of NH to subsequent gas phase

reactions after desorption. In order to resolve the discrepancies of this work and previous studies, we further investigated the impact of gas phase reactions. The gas phase reaction times were varied by adjusting flow velocities and [NH] decays were recorded. Then the measurements were simulated with a computer program "Facsimile" including thirty reactions. The results indicated that, contrary to the work of Umemoto[7], NH was produced on W surface. Also, the results of our simulations and measurements did not preclude NH_2 production on surface.

Based on this study, a new reactor has been designed to produce InN quantum dots on TiO_2 substrate, as shown in Figure 3. Pt/Rh wire will be used to decompose NH_3. The distance between catalyst and substrate can be adjusted to optimize experimental conditions (high radical concentrations and low substrate temperatures). A second inlet perpendicular to the movable NH_3 source will be used to introduce $In(CH_3)_3$ and/or H_2O to avoid their decompositions on hot catalyst. Both inlets are pointing the TiO_2 substrate at 45° angle.

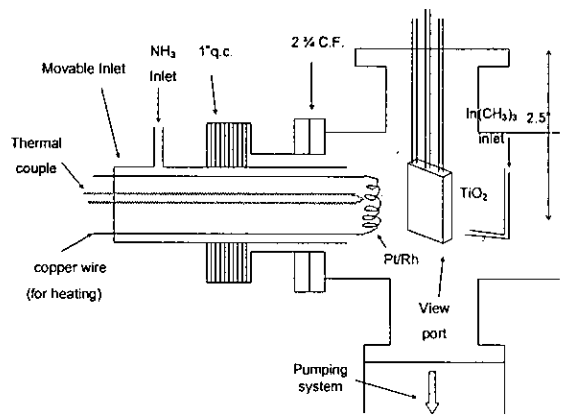

Figure 3. Reactor employed in InN quantum dot production.

二、InN 量子點的製作：

(一) 微波製作 InN / TiO_2 薄膜（李遠鵬、林明璋）：

Figure 1 shows the experimental setup. The reaction chamber is a tubular quartz cross (diameter 5cm) with a sidearm of length = 5cm. A temperature controller (Omega CN9000) regulated the temperature of the reactor through resistive heating. A microwave-discharge system with a flowing gas mixture of NH_3 in He produced the NH_x (x = 2, 1) radicals. TiO_2 nanoparticles were prepared by a method similar to that reported by Zaban and coworkers.

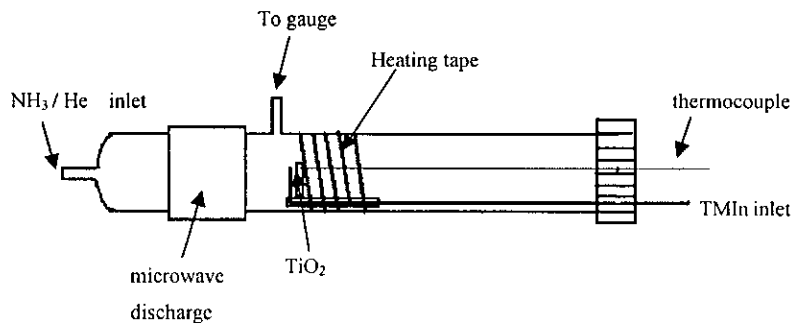

Figure 1. Schematic diagram of the homemade plasma enhanced chemical vapor deposition (PE-CVD) system.

Figure 2 indicates the XRD pattern of InN particles deposited for two hours; the pressure ratio between two reagents were NH_3/TMIn = 800. In the pattern, several different orientations, 100, 002, 101, and 102, of the deposited InN particles and the anatase of the TiO_2 nanoparticles could be identified. No peaks of indium droplets were found in the spectra.

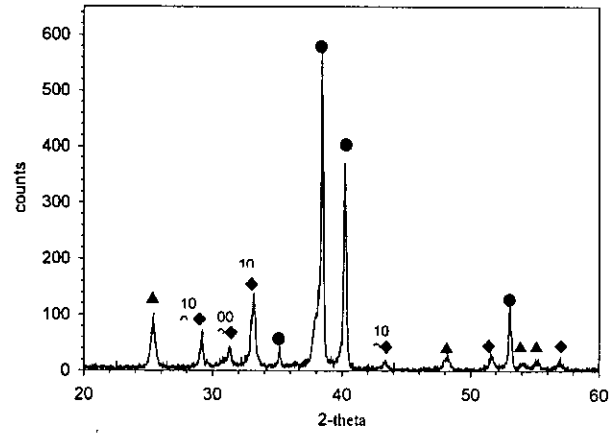

Figure 2. X-ray diffraction patterns for polycrystalline InN on TiO_2 nanoparticles after two-hour deposition processes. ◆: the XRD peaks of InN; ●: the XRD peaks of Ti foil; ▲: the XRD peaks of TiO_2

The SEM morphologies of TiO_2 and InN with a magnification of 35000× are shown in Fig. 3. The TiO_2 nanoparticles formed a smooth and uniform surface before the deposition. After a two-hour deposition, the InN nanoparticles, as confirmed by XRD analysis, showed a ball-like shape. The average particle size of InN is about 100-300 nm.

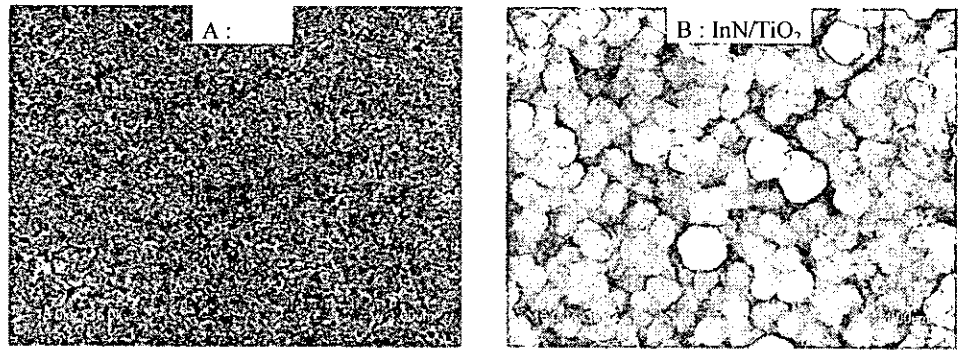

Figure 3. SEM images that show the surface A: before and B: after two-hour InN deposition on TiO_2 nanoparticles, taken with a magnification of 35000×.

The smaller size of InN particles could be performed by reducing the concentration of TMIn, and they have an ability of photovoltaics, the conversion of sunlight to electrical power. Figure 4 shows the relations between irradiation wavelengths and photocurrents. The maximum photocurrent is about 2μA at 380 nm.

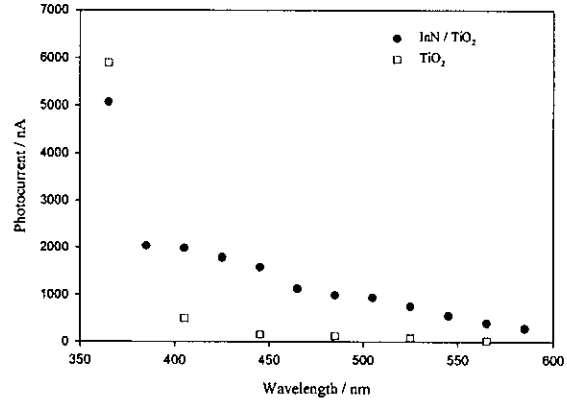

Figure 4. Photocurrent—irradiation wavelength measurement for a InN/TiO_2 cell.

Figure 5 shows the the photocurrent–voltage (I–V) curves of the InN-sensitized solar cells using AcCN-electrolytes. The photovoltaic parameters obtained were V_{OC} = 610 mV, J_{SC} = 0.52 $mAcm^{-2}$, ff = 0.53, efficiency = 0.17 %.

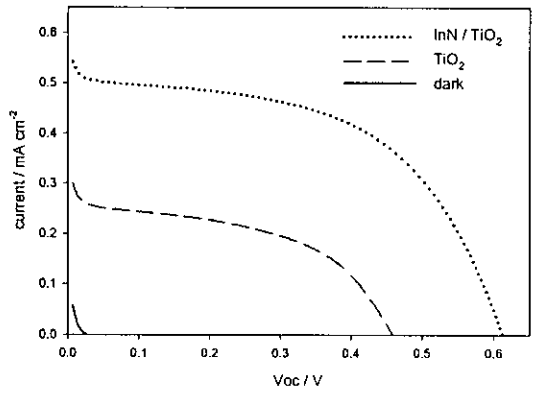

Figure 5. I–V curves of InN-sensitized solar cells based on AcCN-electrolytes (light intensity: 100 $mWcm^{-2}$ AM 1.5).

Unfortunately, the rate of growing InN particles is quick on the surface of TiO_2 film, so that the holes of the porous TiO_2 film are choked up easily with InN particles. It is quite difficult to deposit InN particles in the deep layer of TiO_2 film. The efficiency can not be enhanced, if this problem is not solved. In order to overcome this tough problem, we plan to enlarge the diameter of holes on the surface of porous TiO_2 film by using polystyrene microspheres. The SEM of TiO_2 film with a magnification of 2000× is shown in Fig. 6. Lots of lager holes are formed. The diameters of the holes are about 2μm. However, the quality of this kind of TiO_2 film is not good, because TiO_2 nanoparticles are easily peeling off, and some holes are not opened completely. Therefore, the resistance of the TiO_2 film is quite large, and the photocurrent can not be enhanced. Moreover, the fill factor of the InN/TiO_2 sample also becomes smaller, which is compared with the past results. Thereby, we have to spend some time to modify the TiO_2 film to get much greater results.

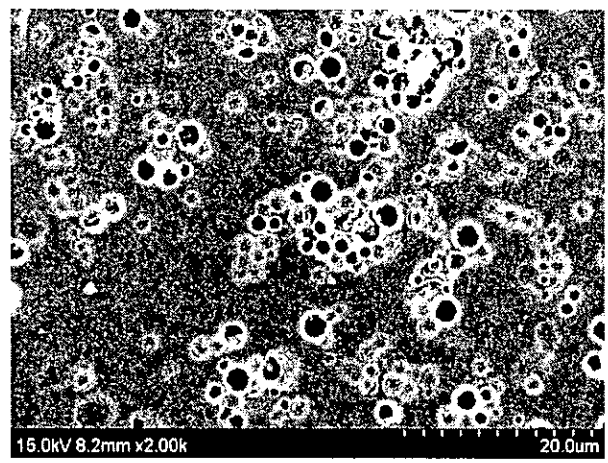

Figure 6. SEM images that show the TiO_2 nanoparticles, taken with a magnification of 2000×.

(二) OMCVD of InN on TiO_2（王載德、林明璋）：

First, we attempted to deposit InN nanoparticles on the TiO_2 thin-film. Figure 1 is the SEM image of InN at different temperatures after 2 hour deposition. We can see that the InN particles with dia. ~40 nm distribute randomly on the TiO_2 surface. The EMAX analysis shows atomic ratio of In nearly constant ~5% at different temperatures whereas no N atoms can be detected. In the XRD spectrum (Figure 2), apparent InN diffraction peaks can be seen at high temperature reaction. However, all these peaks are absent at 310°C deposition. This indicates InN is not crystallized at temperature lower than 350°C. The nearly amorphous structure observed in SEM also supports this result.

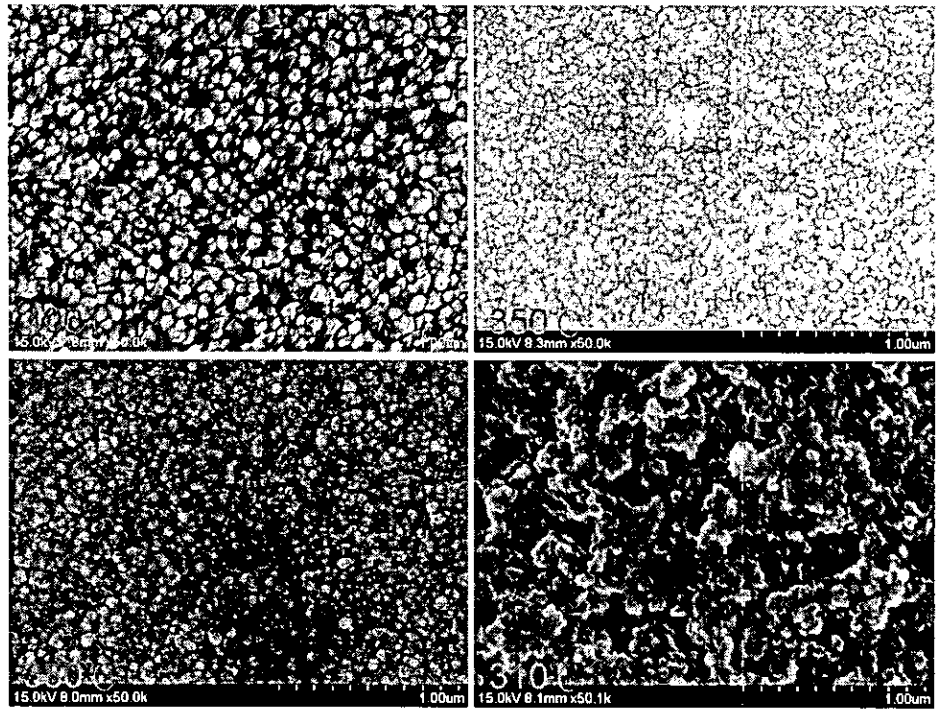

Figure 1. SEM images of InN/TiO_2 after 2hr CVD at 400, 380, 350 and 310°C.

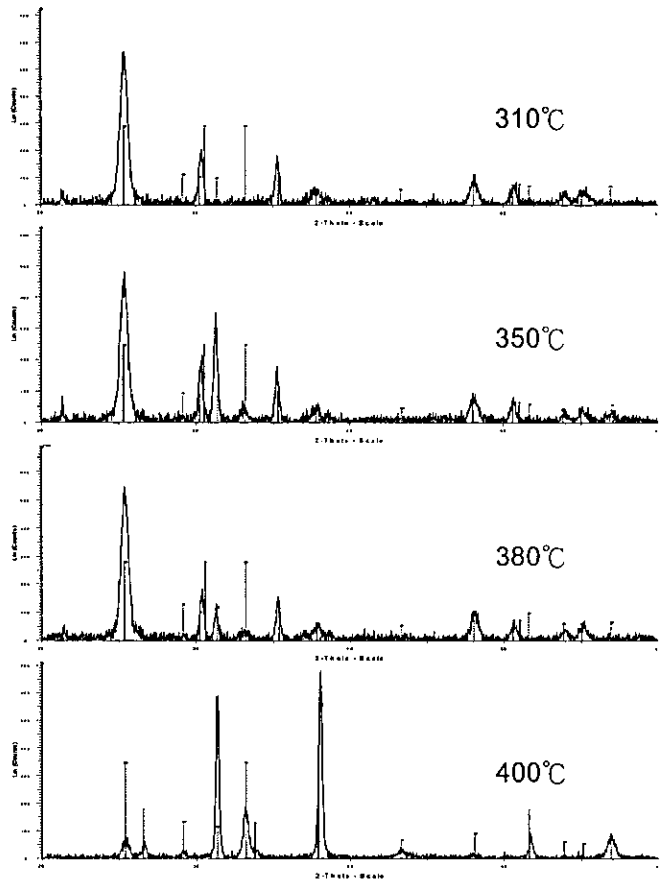

Figure 2. XRD spectrum of InN/TiO_2 after 2hr CVD at 400, 380, 350 and 310°C. (Anatase TiO_2: red, InN: green, ITO: blue)

Somehow, the photocurrent of long time deposition is quite poor and may be attributed to several reasons: First, the defects of InN itself increase with thicker film growth. Second, the cavities of TiO_2 are too small to accommodate InN molecules and the InN molecules simply cover on the "TiO_2 surface". Third, poor connection established between heterospheres of InN, TiO_2 and conducting glass. Therefore, we spin a monolayer untreated TiO_2 sol-gel as a barrier layer (Figure 3); compact bulky structure may improve the electron transfer efficiency to conducting glass greatly. Then, we add w/w 33% M.W. 35,000 polyethylene glycol in the

TiO_2 sol gel after hydrothermal treatment. The polymer would be burned out at 450°C baking with random cavities (Figure 3; dia. ~100nm) left behind. These porosities shall hold the InN molecules more tightly and increase the InN adherent efficiently at high temperature CVD.

Figure 3. The SEM of TiO_2 nanoparticle.

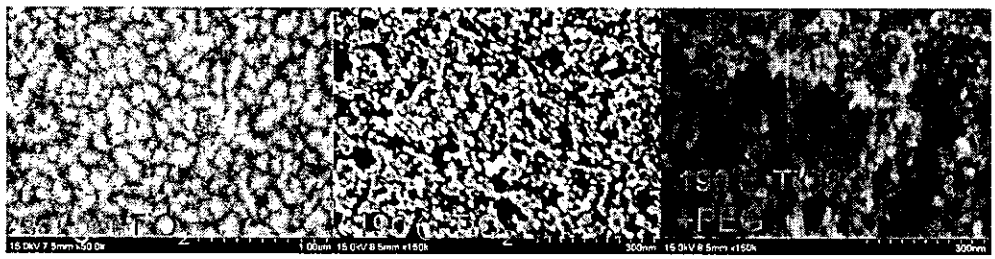

In Figure 4a, we compare blank a TiO_2 mixed with PEG 35,000 autoclaved at 250°C, the results shows that the barrier layers do improve Φ (efficiency) significantly.

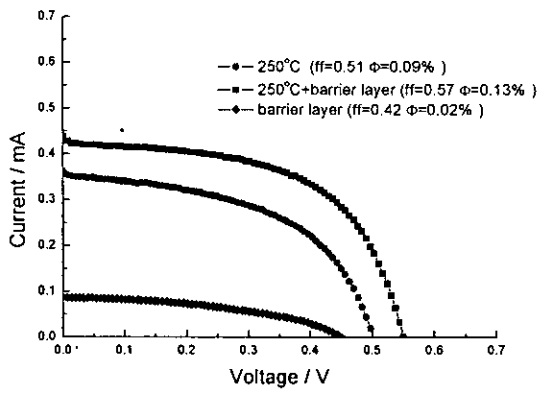

Figure 4a. I-V curve of blank TiO_2/FTO

Figure 4b presents the effect of deposition temperature and deposition time on Φ. The SEM and XRD spectrum shows that InN is crystallized at high temperature as well as longer time deposition. Poorer connection between these two discrete layers causes the I_{sc} and V_{oc} drop greatly.

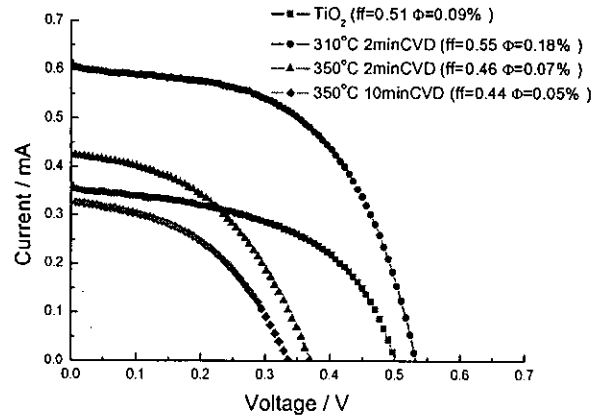

Figure 4b: I-V curve of INER 250°C TiO_2/FTO

With the help of untreated TiO_2 barrier layer, 2 min CVD sample has the highest quantum efficiency so far. In comparison with no barrier layer sample, the InN efficiency is estimated as 0.09%. To modify the TiO_2 surface, we passivate monolayer H_2S over TiO_2 at 120°C. The HS- group shall react with In (TMIn) to become InS. This robust amorphous InS layer also has a great improvement itself. However, when we re-cover InN over it, Φ declines again which means this buffer layer is still vulnerable at high T.

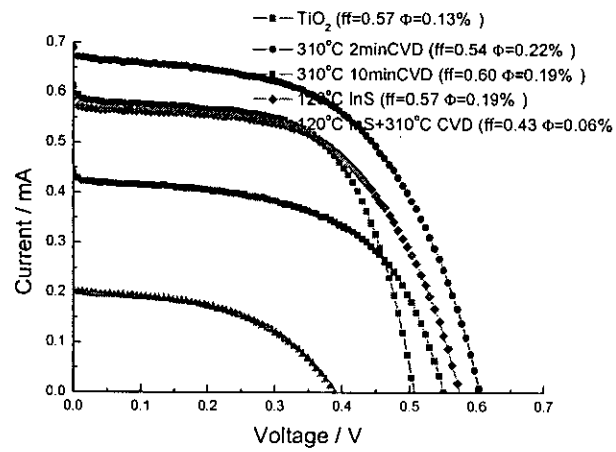

Figure 4c. I-V curve of INER 250°C TiO_2+barrier layer/FTO

(三) Effects of TiO_2 surface modification (王政凱、陳仕燁、林明璋):

1. TiO_2 films

Conducting glass plates(referred as OTE) have to be washed with DI-water, acetone, and ethanol by sonication. Before coating TiO_2, The clean OTE was stored in ethanol.

TiO_2 colloids were prepared by hydrolyzing titanium isopropoxide in a glacial acetic acid solution followed by autoclaving the suspension at 473 K for 12 h. The details of the procedure can be found elsewhere[2-3]. The suspension was applied to the OTE and dried. After annealing these electrodes at 673 K, the average thickness of the film was subsequently measured.

2. Sensitized TiO_2

The TiO_2 films, dried with N_2 purge, were subsequently dipped into a toluene solution of containing quantum dots of conductors and semiconductors such as Au, InTe, AgSe, BiTe. The films were kept immersed for 12h or longer times. Resulting TiO_2 films, adsorbed with semiconductors, were then washed with toluene and dried. After that, these films were put into the PECVD system and covered InN.

3. Growing InN

Indium nitride (InN) was deposited by Plasma Enhanced Chemical Vapor Deposition (PECVD) system, onto TiO_2 surface. NH_3 and Trimethyl Indium are precursors of InN. Different InN thickness, deposition distance and reaction temperature, were varied in this experiment.

4. Sample measurement:

The morphology of InN was examined by SEM. Photocurrent

and open-circuit photovoltages (V_{oc}) were measured using a Keithley 2400 programmable electrometer along with AM1.5 light source. These sample were also analyzed by X-ray diffraction (XRD).

Figure 1 shows the I-V characteristics of different InN deposition times. 60 minute-deposition is better than 30 minute-one in conversion efficiencies. It was formed that longer than 60 minute-deposition samples become worse and worse in fixed flow rate.

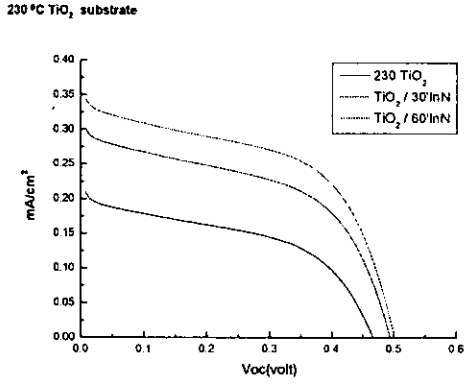

Figure 1

The films dipped into several semiconductor nano-particle solution. Figjure 2 shows the morphology of the TiO_2 surface, adsorbed with Au nano-particles.

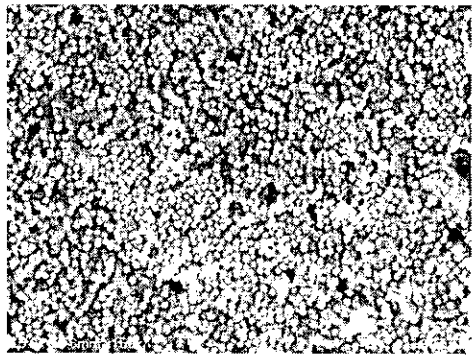

Figure 2

Quantum dots of other semiconductors have also been studied with InN over-coverage; the InN thickness, growing temperature, and deposition distance were all the same, and the enhancement effect can be found in the following figure. Figure 3 shows these semiconductors contribute noticeably to photocurrent and photo-voltages.

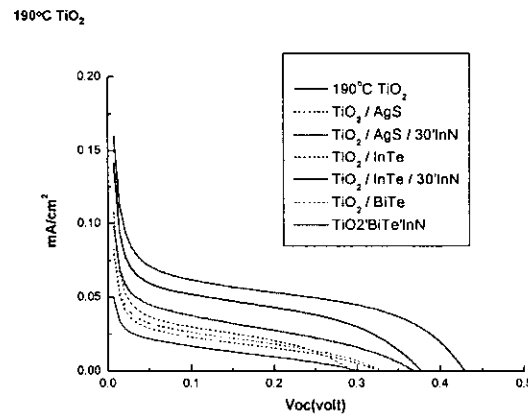

Figure 3

InN powder can also be produced from reactions of NH_x with $In(OH)_3$ at high temperature. The details of the procedure can be found elsewhere. PECVD system can lower the reaction temperature, and rapidly deposit products on the substrate.

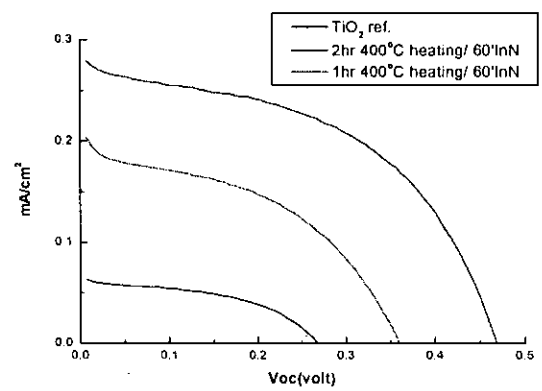

Figure 4

In our experiment, the TiO_2 films were dipped into $In(OH)_3$ solution. The films kept immersed in solution for 12h. After that, the films were washed with DI-water for several times in order to have a minimum amount of $In(OH)_3$ on the TiO_2 surface.

The films, adsorbed $In(OH)_3$, react with NH_x generated by microwave dischange radicals at 400°C for different time and then were covered the same thickness of InN. Figure 4 shows a longer NH_x reaction time provides a better efficiency. The biggest one (red line) is 6 times the efficiency of the TiO_2.

(四) Syntheses of metal chalcogenide nanoparticles and morphology control syntheses of anatase TiO_2 nanocrystals (李積琛、林明璋):

Recently, the composite films containing TiO_2 and InP nanoparticles have shown a strong photoconductivity in the visible region, which can be utilized for conversion of solar energy into electrical power with a photoelectrochemical cell. Our approach to enhancing the response of the solar cell is based on replacing the dye with nanoparticles of semiconducters, followed by covering a thin layer of InN to protect the sensitizer and enhance the photocurrent. The objective of this research is the preparation of a high-efficiency solar cell using quantum dots of semiconding materials as the senstizer on metal oxide film to fabricate thin film solar cell (Figure 1). Our studies have been focused on the preparation of semiconductor nanomaterials in varies binary systems and TiO_2 anatase nanoparticle and nanorod films. In this report we discuss our progress in: 1) Synthesis of binary chalcogenide nanoparticles: The goal of this study was to

produce a stable semiconductor nanoparticles to produce a material capable of absorbing visible light that will be used as the inorganic sensitizer on photovoltaic solar cell device. 2) Morphology control of TiO_2 nanocrystals to study the effect of TiO_2 crystal shape to photo response of solar cell and 3) Thin films of M_xX_y/TiO_2 (M = In, Bi; X = Se, Te), and 4) photocurrent measurement of solar cell device using the as-prepared thin films [8-11].

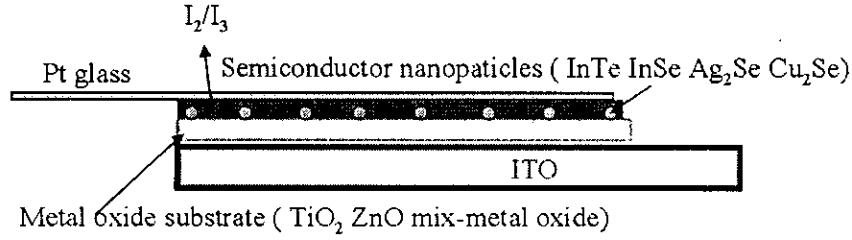

Figure 1. The schematic illustration of a thin film solar cell.

1. Solution Method for the Preparation of Metal Chalcogenide Nanoparticles [12-14]:

Nanoparticles of low band gap binary chalcogenide semiconductors were prepared using the colloid solution method. The surfactant (TOP/HDA) was used as the capping agent to synthesize nanoparticles in a particle size range 5-20nm. In this year, we have successfully synthesized In_2Te_3, In_2Se_3, Cu_2Te, Ag_2Te nanoparticles. In_2X_3 (X = Se, Te) nanoparticles were prepared by mixing a solution of $InCl_3$ (or $In(ac)_3$), Se (or Te) element in solution of TOP/HDA. The mixed solution was heated for 24 h at 250°C under nitrogen atmosphere. Formation of the In_2X_3 nanoparticles is accompanied by the appearance of an intense brown color. The as-synthesized nanoparticles were

diluted with toluene and precipitated with methanol. The precipitate was dissolved in pyridine and precipitated again in an excess amount of methanol. M_2Se (M=Cu, Ag) nanoparticles were prepared by mixing a solution of MNO_3 (M=Cu, Ag), SeO_2 and $NaBH_4$ in solution of toluene. The mixed solution was heated for 24 h at 250°C under nitrogen atmosphere. Formation of the In_2X_3 nanoparticles is accompanied by the appearance of an intense color. The resulting black suspensions were centrifuged and the precipitates were washed three times with absolute methanol. The as-synthesized nanoparticles were diluted with toluene and precipitated with methanol. The precipitate was dissolved in pyridine and precipitated again in an excess amount of methanol (Figure 2).

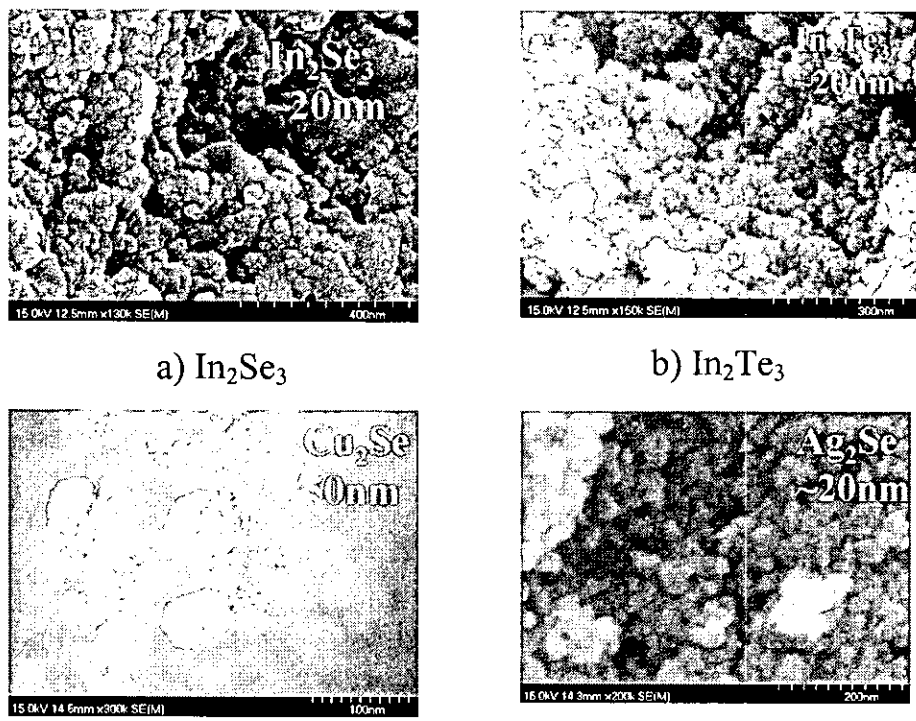

a) In_2Se_3 b) In_2Te_3

c) Cu_2Se d) Ag_2Se

Figure 2. SEM images of a)In_2Se_3, b) In_2Te_3, c) Cu_2Se, d) Ag_2Se

2. Morphology control of TiO_2 nanocrystals [15-17]:

Nanocrystalline TiO_2 in anatase form was synthesized via a combined sol–gel process with hydrothermal treatment. In a typical synthesis, a specified amount of 2-propanol (10 ml) was first introduced into $Ti(OR)_4$ (37ml). The mixed solution was then gently added drop wise into a solution of water (250 ml) and acetic acid (80 ml) under N_2 flow. The solution became pale blue solution after the process was done. The mixture was continuously stirred at 80°C 3 hrs to obtain white sol. Then, the gel was cooled to room temperature to become pale blue, transparent solution. Subsequently, the gel was dried at 80°C 3 hrs, the dried sample was calcined at 500-700°C for 1-24h to produce the desired mesoporous TiO_2 photocatalyst. TiO_2 nanorods with were synthesized by a hydrothermal treatment procedure. The anatase form of TiO_2 powder (2g) was put in 10 M NaOH (100ml) and autoclaved at 130°C for 24 h. After cooling to room temperature, TiO_2 nanorods were suspended in 0.01 M HCl solution for 30 min, filtered, and repeated the same procedure for several times to remove excess NaOH. As a final step, the sample was dried at 100 °C for 3 hrs. X-ray diffraction was used to confirm the anatase TiO_2 polymorph with a small amount of sodium titanate (Fig. 3).

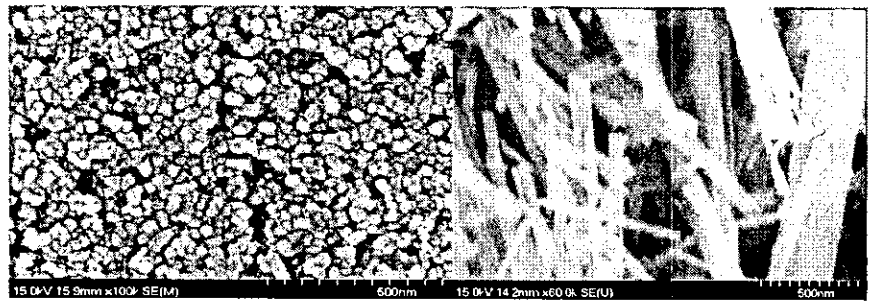

a) TiO_2 nanoparticles b) TiO_2 nanorods

Figure 3. SEM images of TiO_2 nanocrystals a) nanoparticles, b)nanorods

3. Characterization:

X-ray diffraction was used to confirm the purity of each product. The morphology of these as-synthesized nanoparticles were examined by SEM and TEM. These nanoparticles will be deposited on the metal oxide film to study the effect of particle size to the photocurrent of the solar cell using a AM1.5 solar simulator.

Results

1. The effect of semiconductor nanoparticles on photocurrent:

Solar cell devices with films of M_xX_y/TiO_2 (M = In, Bi; X = Se, Te) have been fabricated. Photocurrent measurements (Figure 4-6.) show significant photocurrent response under a AM1.5 solar simulator for each sample. The film with In_2Te_3 nanoparticles exhibits the most pronounce photocurrent, especially in wavelength range 600-700 nm. When a small amount of ZnO nanoparticles was introduced to the film, the photocurrent increased (Figure 4). Additional experiment on the deposition of InN on top of the In_2Te_3/TiO_2 film shows even higher photocurrent. The preliminary studies indicate that the InN layer can improve the photocurrent of thin film with $InN/In_2Te_3/TiO_2$ (Figure 5).

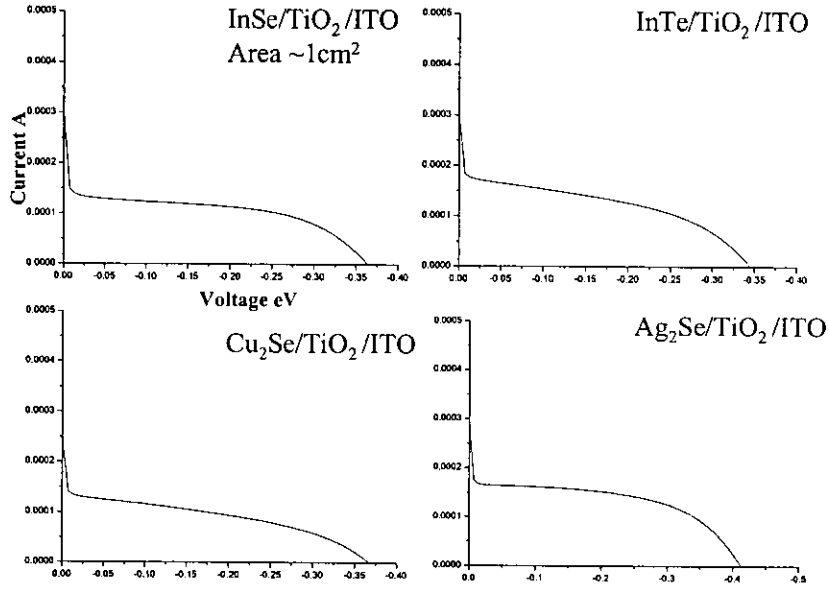

Figure 4. I–V curves of semiconductor-sensitized solar cells based on films of a)In_2Se_3/TiO_2, b)In_2Te_3/TiO_2, c) Cu_2Se/TiO_2 and d) Ag_2Se/TiO_2. (electrolytes: I_2/I^- solution; light intensity:100 $mWcm^{-2}$ AM 1.5).

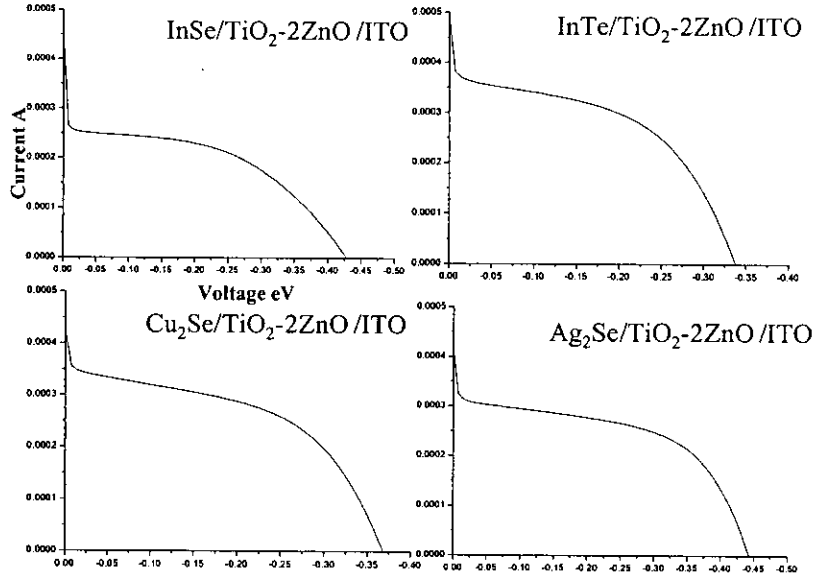

Figure 5. I–V curves of semiconductor-sensitized solar cells based on films with ZnO nanoparticles a)In_2Se_3/TiO_2-2ZnO, b)In_2Te_3/ TiO_2-2ZnO, c) Cu_2Se/ TiO_2-2ZnO and d) Ag_2Se/ TiO_2-2ZnO. (Electrolytes: I_2/I^- solution; light intensity:100 $mWcm^{-2}$ AM 1.5).

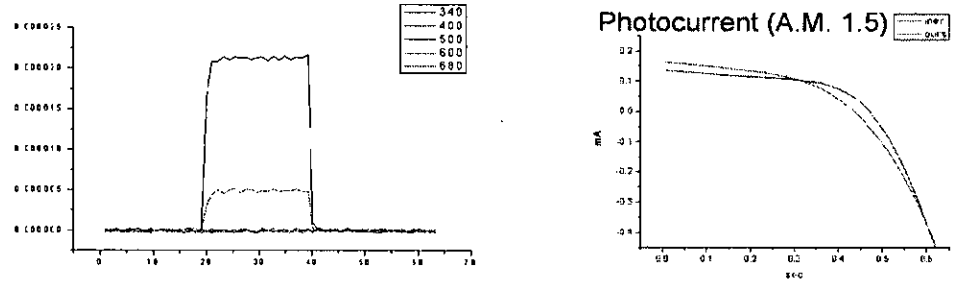

a) b)

Figure 6. a) Photocurrent of TiO_2 film in different wavelength. b) I–V curves of solar cells based on TiO_2 film. (Electrolytes: I_2/I^- solution; light intensity:100 $mWcm^{-2}$ AM 1.5).

2. Synthesis of TiO_2 nanoparticles and nanorod:

The preparation of anatase form of TiO_2 nanoparticles and nanorods has been made. Powder x-ray diffraction pattern of TiO_2 nanoparticle shows pure anatase form and the nanorod sample exhibits small amount of impurity sodium titanate. The photocurrent measurements of blank TiO_2 film (nanoparticle) reveals similar results to samples from INER, indicating high quality of TiO_2 film can be prepared in NCTUAC (Figure 6). The photocurrent study to TiO_2 nanorod film is in progress.

三、TiO_2 基板的製作：

(一) Tereza Paronyan、林明璋：

1. Experimental

(1) Synthesis of nanocrystalline TiO_2 colloids

A. Precipation (hydrolysis of Ti-alkoxide using glacial acedic acid).

Titanium(IV) isopropoxide (37ml) and 2-propanol (10ml) mixture was rapydly added to 0°C disstilled water (250ml)

conaining 80ml glacial acedic acid with stirring. White precipitate formed immediately uppon addition of the titanium (IV) isopropoxide and 2-propanol solution [18].

B. pH varying to pH = 1

After precipitation in the reaction solution was added 2 ml conc. HNO_3 with stirring to reach pH = 1

C. Peptization (heating at 80°C for 8h)

D. Hydrothermal growth/autoclaving(12h, 190-230°C)

Autoclaving of these sols allow controlled growth of the primary particles and also the extent of the crystallites. The pore size distribution of the film depends on the aggregate size and distribution. At the temperature range, it can provide anatase crystalline nanoparticles, at higher autoclaving tempertures, more rutile formation occurs.

E. Sonication (ultasonic bath, 250W, 15x3 sec)

Sedimentation takes place to some extent during the hydrothermal growth procedure and the precipitates are redispersed using ultrasonic bath.

F. Concentration (45°C, 30 mbar). The sol is then concentrated at 45°C on a rotary evaporator to reach a final concentration of ca. 11%.

G. Binder addition: NH_3 aqueous solution was used also for providing the porosity in the TiO_2 film.

An increase in the porosity of the film can be obtained by adding a binder such as polyethylene glycol (M_w 20000) or ethyl cellulose in ethanol mixed with terpineol.

(2) TCO substrate cleanning

To clean TCO substartes is important for providing good mechanical and electrical contact with TiO_2, low resistivity (10-70 Ω/square) and ~80% light transmission.

ITO-In_2O_3:SnO_2 (dopant) and FTO- SnO_2: F (dopant) substates were used as TCO material.

Cleaning of TCO substrates was carried out in the ultrasonic bath with acetone, ethanol, detergent, dioniz. water, ethanol, UV/Ozone cleaner.

(3) TiO_2 compact film deposition by spray pyrolysis

To reduce dark current losses due to short circuit of electrons on the TCO substrates the TiO_2 compact film was deposited by spray pyrolysis using TAA (Di-iso-propoxy titanium bis(acetylacetonate) $((CH_3)_2CHO)_2Ti(C_5H_7O_2)_2$ as source of titanium dioxide[19] or before nanoporous film deposition the substrates immerse in 0.05-0.1M $TiCl_4$ aqueous solution.

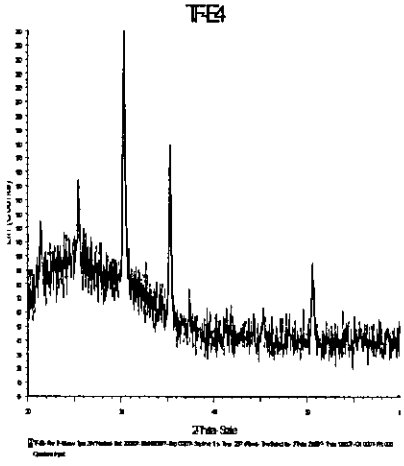

Pict 1. XRD patterns of 0.02M TAA pyrolysis on ITO substrates.

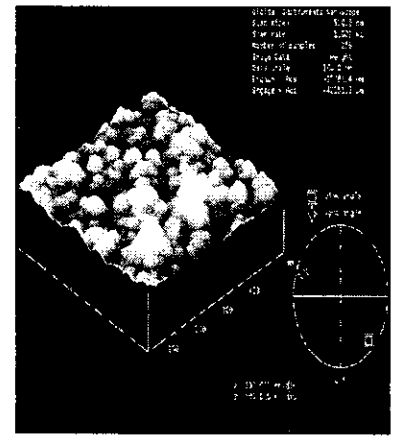

Pict.2. AFM images of film surfaces deposited from 0.2M TAA solution.

Pyrolysis of TAA aerosol was performed on the TCO substrates under varying experimental conditions and source concentration. The optimized procedure was as follows: 0.2M TAA solution was sprayed layer by layer from distance 15cm onto the hot substrates whose temperature was kept 450°C using chromatographic atomizer. Each next portion of the aerosol was applied after 30sec. pause, necessary to complete the pyrolysis of the previous layer. Finally the prepared TCO/TiO_2 electrodes were annealed at 450°C (for ITO), 500°C (for FTO) 30min.

The XRD analyisis and AFM images patterns were carried out after annealing of TiO_2 films. The thickness of compact film was controlled by spray time and distance. Average thickness of films was 70-120 nm.

The TCO substrates treatment in the $TiCl_4$ aqueous solution was carried out at the 70^0C 30 min. After treatment the samples were dried at 100^0C and used for coating of TiO_2 nanoparticles containing concentrated gel.

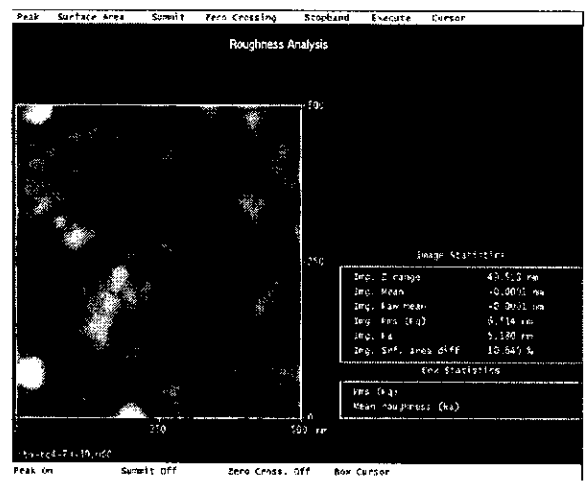

Pict.3 AFM surface image ITO substrate after treatment in the 0.1M $TiCl_4$ aqueous solution at 70^0C for 30 min.

(4) TiO_2 nanoporous film preparation and characterization

Nanocrystalline titanium dioxide colloid is ready (2.1) for deposition on the conducting glass substrates which was covered already with compact layer (2.3).

The sol is deposited by the spin coating and doctor blade methods. For the thinner layer preparation (~1μm) was used the spin coating method. The spinner regime usually was I step-speed/2000 rpm/30sec and II step- speed/3000 rpm/60sec. After each sprayed layer (~100nm thicknesses) the films were heated at 100°C. To provide contact area for future I-V measurements was used Scotch tape which can control the thickness of gel when for coating was used with the doctor-blade technique. The films are then dried in air about 10min and fired at 450°C 60min (for ITO) and 500°C 60min (for FTO), because ITO surface is very sensitive on oxygen and increasing the the resistivity of ITO films at higher temperatures. The optimal conditions of film treatment can provide bulk crystal structure of anatase crystals, porosity, microstructure, surface area, physical properties and to avoid contamination due to carbon inclusions. The XRD, AFM and SEM analyses were carried out with TiO_2 nanoporous films after annealing for investigations of the nanoparticles crystal structure, sizes, porosity and surface. I-V measurements were investigated under different light wavelengths using Kethley 2440 sourcemeter and xenon lamp (1kw) for light source.

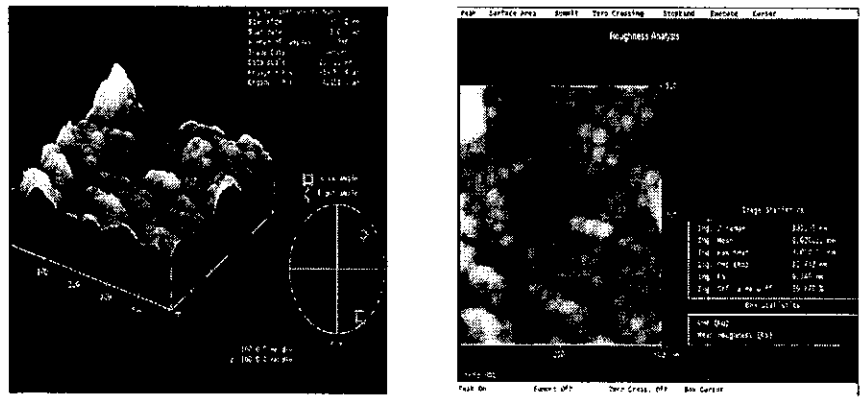

Picture 4. AFM images of TiO_2 nanoporous films, avarage size of nanoparticles is 20nm.

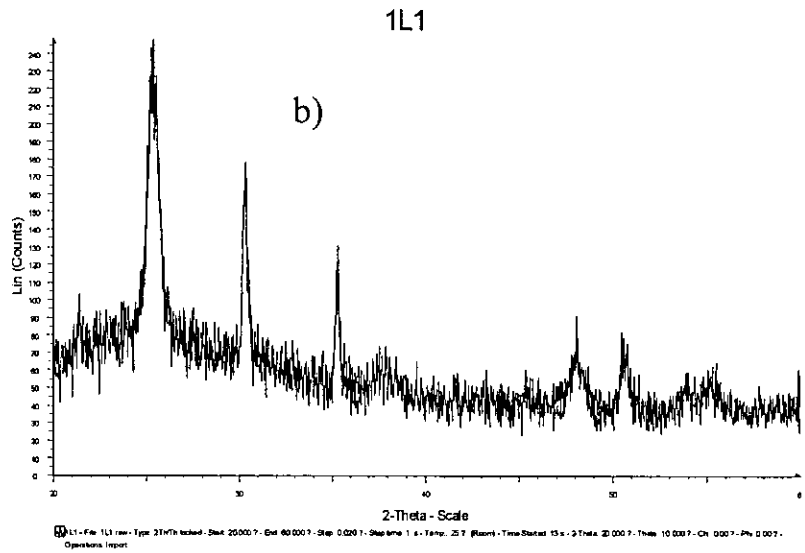

Picture 5. XRD patterns of TiO_2 nanoporous films film thickness ~100nm, with anatase peaks, ITO peaks also appeared on the patterns

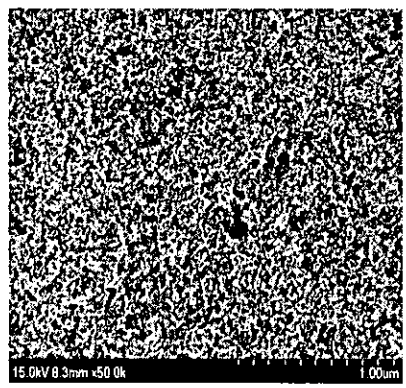

Picture 6. SEM images of TiO_2 film surfaces, synthesized at 450°C, 60 n the ITO substrates.

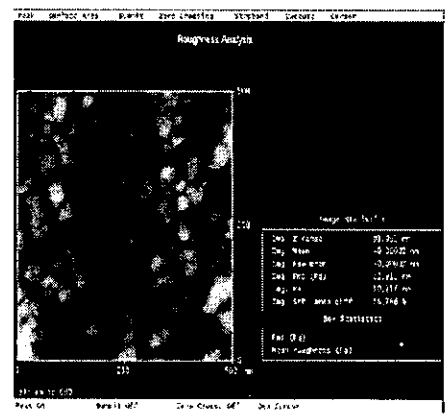

Pict. 7 AFM image of TiO_2 nanoporous film after addition NH_3.

(5) TiO_2 surface treatment

Studies have shown that deposition of a secondary oxide layer to the nanotextured film improves significantly the cell performance. In one procedure the film is impregnated with $TiCl_4$ by immesing the film in a solution in ice water followed by firing at 450°C for 30 min.

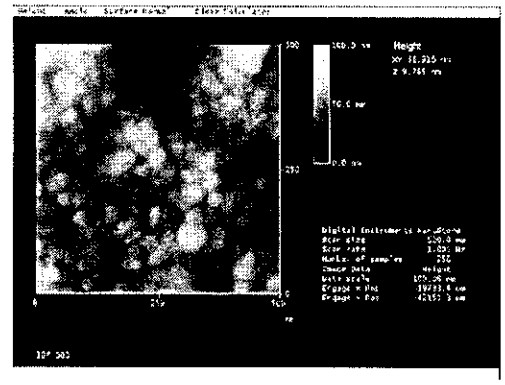

Picture 8. AFM images of TiO_2 nanoporous film after $TiCl_4$ treatment without annealing

(6) I-V characterization of TiO_2 photoelectrode

The I-V characteristics were carried out using Keithley 2400 Sourcemeter and 1kW xenon lamp (1kW). The electrolyte was I^-/I_3^- redox system, prepared from 0.3M LiI and 0.03M I_2 in acetonitrile, counter electrode was Pt wire on the ITO glass substrate.

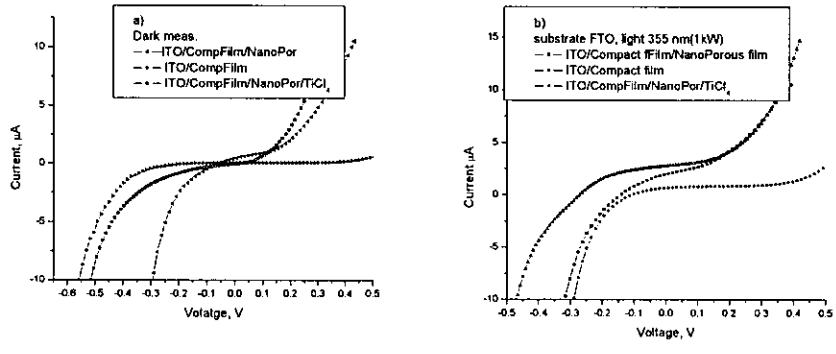

Pict.9 I-V characteristics of TiO_2 photocatalist. a) dark measrumemts, b) under 355nm light (1kW)

2. Dye sensitized solar cells preparation and characterization

Prepared TiO_2 photoelectrodes (already described) have been immersed in the 0.005M N3 (N719) (solarinix, Switzerland). The N719 dye solution was prepared in a mixed solvent of 1:1 acetonitrile tert-butanol. The samples were kept in the dark 24 hours. The sandwich-type solar cell was assembled by placing a platinum-coated conducting glass (counter electrode) on the N719 dye sensitized photoelectrode (working electrode) and clipped together as open cells for measurements. Different redox electrolytes were used for investigation of standart deviations of the I-V parameters (I_{sc} short-circuit photocurrent density, V_{oc} open-circuit voltage, η efficiency, FF fill factor).: 0.3M LiI, 0.03I_2 in acetonotrile, 0.3MLiI, 0.03M I_2. 0.5M 4-tertbutylpiridine in acetonitrile+valeronitrile (5:1), 0.3M LiI, 0.03M I_2, 0,5M 4-tertbutylpiridine, 0.1M guamdinium thiocyanate in acetonitrile + valeronitrile (5:1) and 0.7M tetrabutylammonium iodide (TBAI), 0.01M I_2, 0.5M 4-tertbutylpiridine (TBP) in acetonitrile + valeronitrile (5:1).

A cell of areas 0.3-0.7cm^2 were investigated under sun light using AM1.5 simulator.

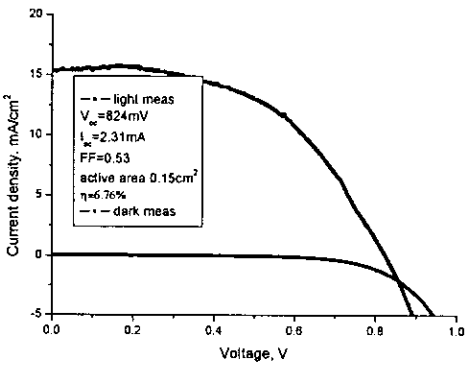

Pict. 10 Photocurrent-voltage characteristics of cell, redox electrolyte was 0.7M TBAI, 0.01M I_2, 0.5M 4-TBP in acetonitrile+valeronitrile(5:1).

The redox electrolyte role is very important to reach higher V_{oc} and the presence the TBA^+ in the electrolyte solution can increase it to V_{oc}= 0.9 V to reach higher conversion efficiency, however there is problem with the Fill factor, for good solar cell it has to be 0.7-0.85.

The surface morphology of TiO_2 nanoparticles influences on the FF and I_{sc} and in the recent article Japanese coworkers confirmed it [20], the surface treatment in 0.1M HCl after $TiCl_4$ treatment can reach 10% efficiency on 0.5 cm^2 cell area.

3. Conclusion

6.8% conversion efficiency was achieved under illumination by simulating AM1.5 solar light (100mWcm^2) :0.36 cm^2 cell surface area, FTO/TiO_2 compact film/TiO_2 nanoporous film/$TiCl_4$ treatment photoelectrode immersed in the $5 \cdot 10^{-3}$M concentration N719 dye..

(二) K. W. Sun (孫建文)：

1. Five different recipes of P-25 solution were prepared. After stirring and grinding for about 30 mins, the solution was spun on glass slides. The morphology of the spin-on TiO_2 particles was studied with an AFM and an optical microscope.

Recipe 1 : P-25 3g +H_2O 5ml+acetylacetone 0.1ml + TritonX-100

AFM image

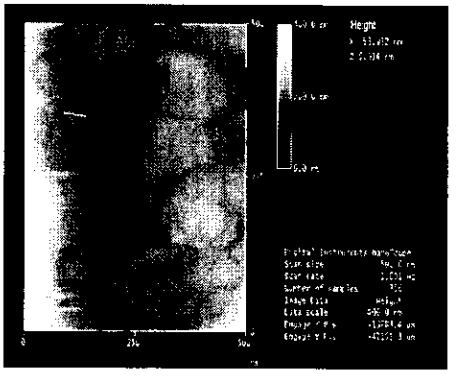

optical image

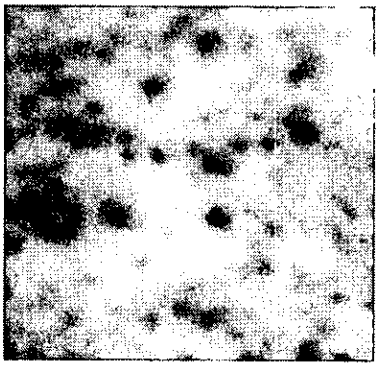

Recipe 2: P-25 3g+ethanol proper +acetylacetone 0.1ml +TritonX-100stir

AFM image

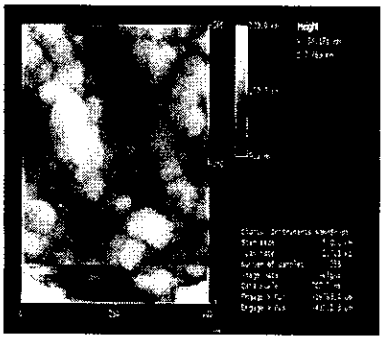

optical image

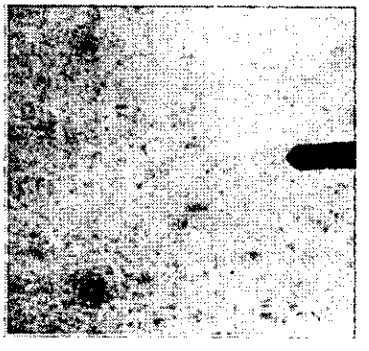

Recipe 3 : P-25 3g+acetone proper+acetylacetone 0.1ml +TritonX-100

AFM image

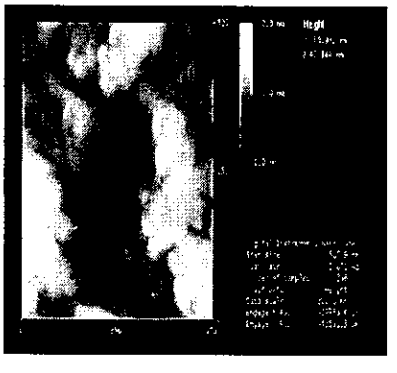

optical image

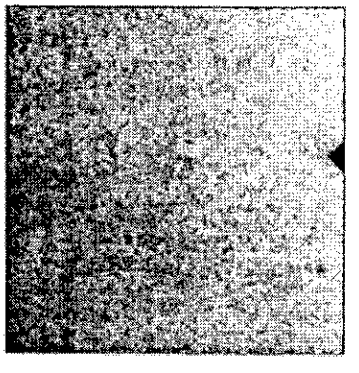

Recipe 4 : p-25 3g+10ml acetylacetone+ethanol proper +tritonX-100

AFM image optical image

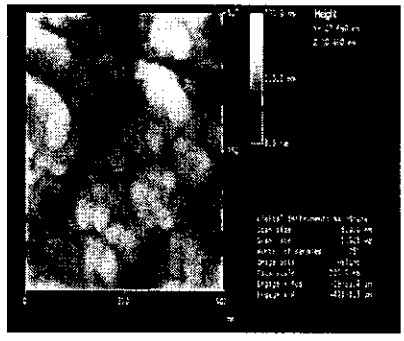

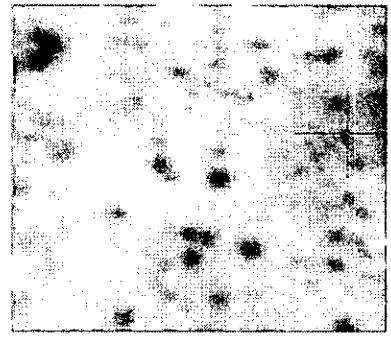

Recipe 5 : p-25 3g +2ethyl-1-hexanol proper +tritonX-100

AFM image optical image

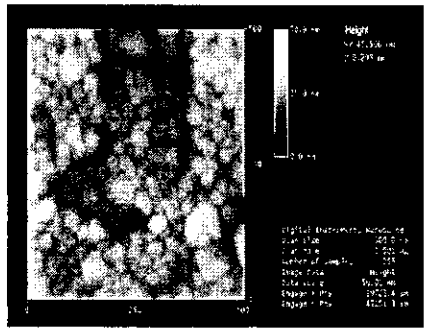

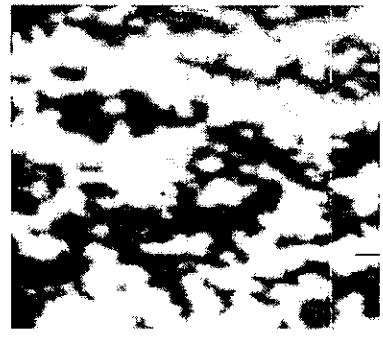

The concentration of the solution can not be easily controlled. We also found that the TiO_2 particles could easily form large clusters and were not able to stick well enough on the glass slides. However, situation improved a bit when we mixed H_2O and ethanol together. The overall particles were still larger than 75 nm. But 2ethyl-1-hexanol can made size range to 45-60nm.

2. In this part of work, only one solution was used in preparing the paste. However, we have mixed different acids in the final

solution. Eight different recipes of P-25 solution were made. After stirring and grinding for about 30 mins, the solution was spin-coated on glass slides. The morphology of the spin-on TiO_2 particles was studied with an AFM and an optical microscope.

Recipe 1: P-25 3g + 0.1M Acetic acid 8ml+acetylaceton 0.1ml+TritonX-100

AFM image optical image

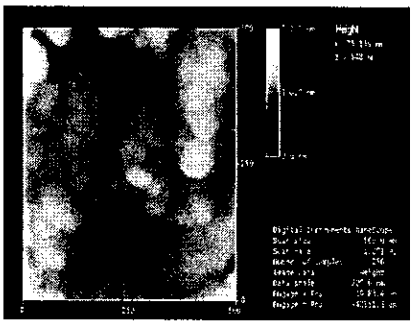

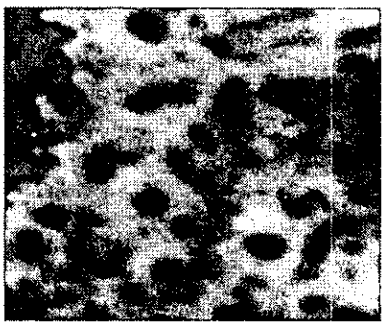

Recipe 2: P-25 3g + 1M Acetic acid 8ml+ acetylaceton 0.1ml+TritonX-100

AFM image optical image

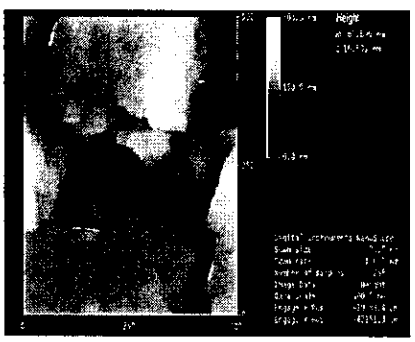

Recipe 3: P-25 3g + 0.1M HNO_3 8ml+acetylaceton 0.1ml +TritonX-100stir

AFM image optical image

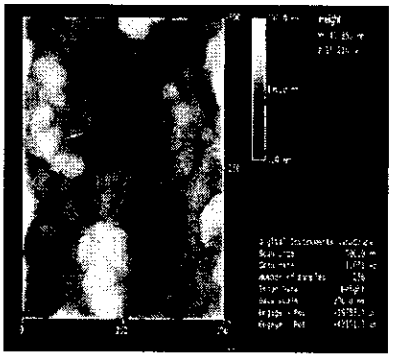

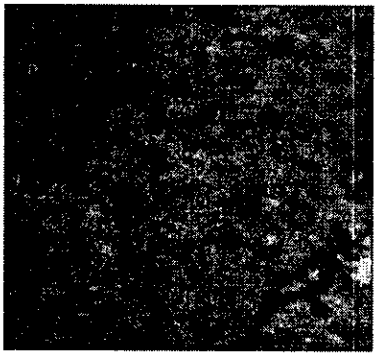

Recipe 4: P-25 3g + 1M HNO_3 8ml+acetylaceton 0.1ml + TritonX-100

AFM image optical image

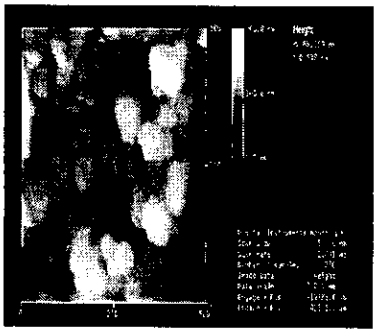

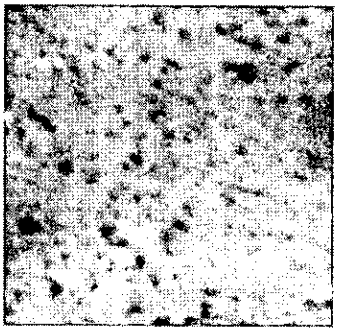

Recipe 5: P-25 3g + dilute NH3 8ml+acetylaceton 0.1ml + TritonX-100

AFM image optical image

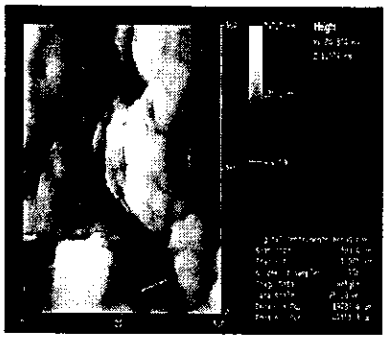

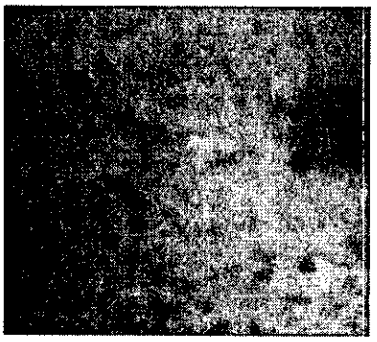

Recipe 6: P-25 3g + dilute NH_3 8ml (dilute again) + acetylacetone 0.1ml+TritonX-100

AFM image optical image

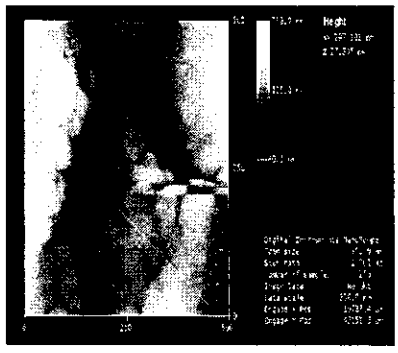

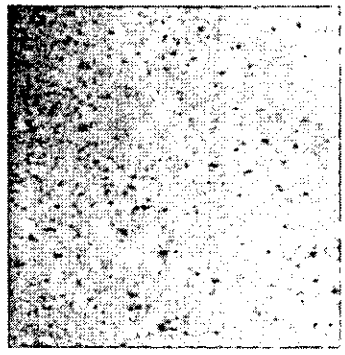

Recipe 7: P-25 3g + 0.08g 4-hydroxy-benzoic acid + acetylaceton 0.1ml+TritonX-100

AFM image optical image

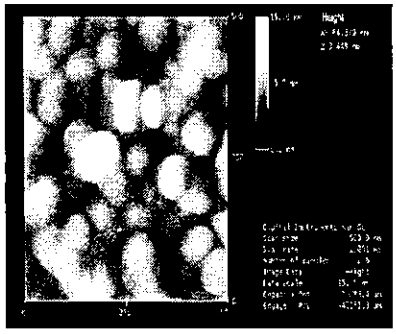

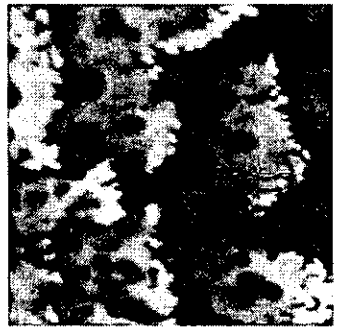

Recipe 8: P-25 3g + 0.23g 4-hydroxy-benzoic acid + acetylaceton 0.1ml+TritonX-100

AFM image optical image

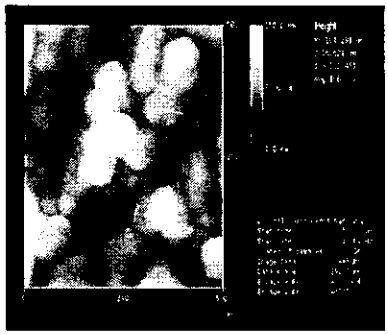

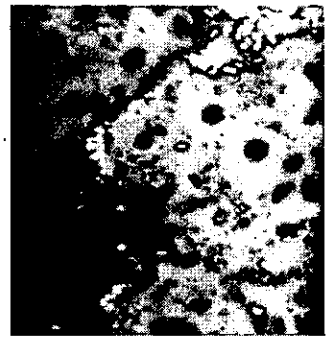

The templates all look quite opaque. And the average particle size was still much large than 25 nm.

3. In this part of work, only one solution was used in preparing the paste. However, we have added 10ml ethanol and mixed different acids in the final solution. Five different recipes of P-25 solution were made. After stirring about 4 days, the solution was spin-coated on glass slides. The morphology of the spin-on TiO_2 particles made from three of the recipes was studied with an AFM and an optical microscope.

Recipe 1:P-25 3g+0.1M Acetic acid 100ml+ acetylacetone 1ml+ethanol 10ml + TritonX-100

AFM image optical image

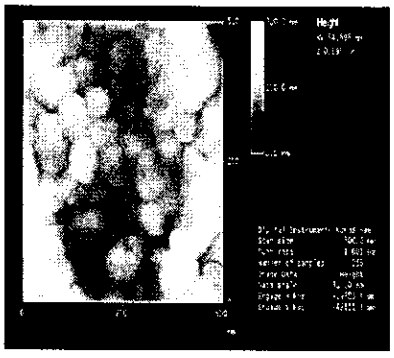

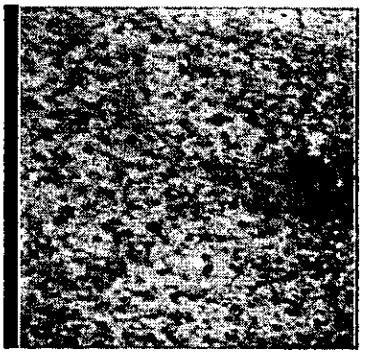

Recipe 2:P-25 3g+0.1M HNO_3 100ml+ acetylacetone 1ml+ethanol 10ml + TritonX-100

AFM image

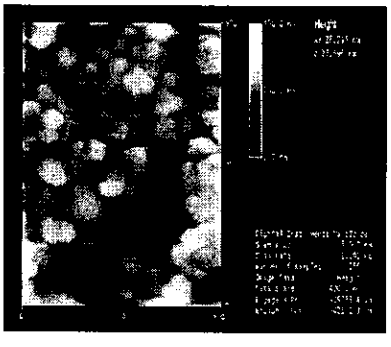

Recipe 3:P-25 3g + 0.1M Formic acid 8ml+10ml ethanol+ acetylacetone 0.1ml +TritonX-100

AFM image optical image

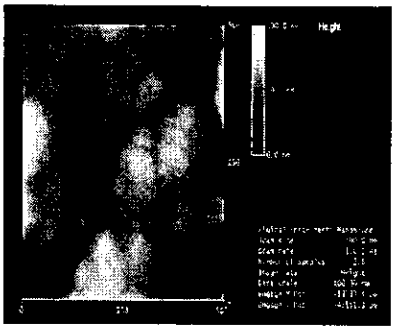

No AFM and optical image for :

Recipe 4:P-25 3g+1M Acetic acid 100ml + acetylacetone 1ml+ethanol 10ml + TritonX-100

Recipe 5:P-25 3g+1M HNO3 100ml + acetylacetone 1ml+ethanol 10ml + TritonX-100

We saw some improvement on the clearance of the film. The templates look semi-opaque. And the particle size was become small than recipes in Part B (especially in compared to recipe 2 in Part B). The particle size range was 20-45nm. The template prepared with the recipe 3 gives the best result from DSC efficiency measurements.

4. Result

Recipe 1 : P-25 3g +H_2O 5ml + acetylacetone 0.1ml + TritonX-100

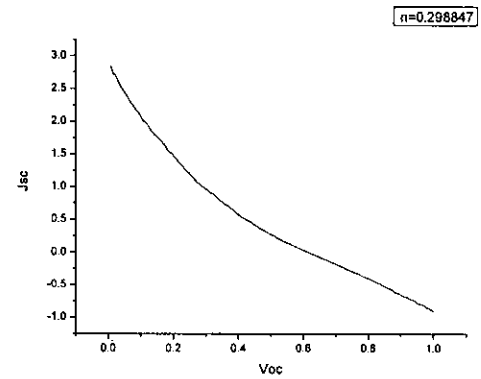

η=0.30 %

Recipe 2: P-25 3g+ethanol proper +acetylacetone 0.1ml +TritonX-100stir

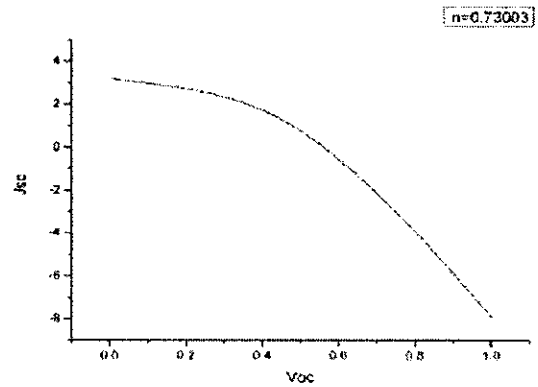

η=0.77 %

Recipe 3:P-25 3g+1M HNO_3 100ml + acetylacetone 1ml+ethanol 10ml + TritonX-100

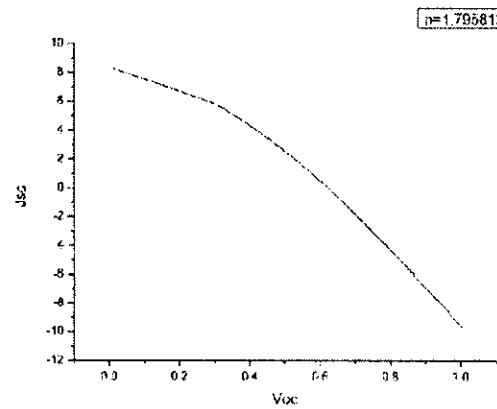

η=1.80 %

In conclusion, well dispersed nanoparticles can have larger surface area and show enhancement in the electrical transport properties. This also justified from the better efficiency measured from DSC with transparent TiO_2 film.

參、主要發現與結論

自去年底發現光電流以來，InN/TiO_2 奈米薄膜系統的光電效率已增進 10-100 倍左右，效率的改進在於 TiO_2 薄膜品質的改進以及 InN 量子點製作技術的逐步修改；再者，在 InN 及 TiO_2 層間加入 In_2S_3, InS_x 薄膜, InTe 等等，均有效率改進的現象。如何增進 InN 及層間的奈米及 TiO_2 量子點的接連是一個重要的課題，此外，如何增加 InN 量子點的數目，亦是很重要的研究方向。

這幾個相關的問題將由 TiO_2 薄膜表面處理著手，諸如利用 $M(OH)_x$ 膠狀溶液(M=In, Ti, Al, B, P,...)覆蓋 TiO_2 薄膜後，再以熱、光或電漿處理，活化 TiO_2 表面，增加活化吸附點，以促進 InN 之成長，未來一年期望可達到目前 0.2%光電效率 10-20 倍左右的目標。

肆、參考文獻

1. J. H. Wang and M. C. Lin, ChemPhysChem, **2004**, 5, 1615.
2. A. Hagfeld, M. Graetzel, Chem. Rev., **1995**, 95, 49; M. K. Nazeeruddin, P. Pechy, M. Graetzel, Chem. Comm., **1997**, 18, 1705; M. Graetzel, Nature, **2001**, 414, 338.
3. O. Khaselev and J. A. Turner, Science, **1998**, 280, 425.
4. Zaban, O. I. Mic´ic´, B. A. Gregg, A. J. Nozik, Langmuir, **1998**, 14, 3153-3156.
5. J. M. Nedeljkovic´, O. I. Mic´ic´, S. P. Ahrenkiel, A. Miedaner, A. J. Nozik , J. Am. Chem. Soc., **2004**, 126, 2632-2639.
6. H. Umemoto et al. Jpn. J. Appl. Phys., **2003**, 42,5315.
7. G. S. Selwyn et al. J. Phys. Chem., **1982**, 86, 760.
8. ÓRegan, B.; Grätzel, M. Nature, **1991**, *353,* 737.
9. Kalyanasundaram, K.; Gra¨tzel, M. Coord. Chem. ReV., **1998**, *77,* 347.
10. Nozik, A. J. Inorg, Chem., **2005**, 44, 6893.
11. Zaban, A.; Mićić, O. I.; Gregg, B. A.; Nozik, A. J. Langmuir**, 1998**, 14, 3153.
12. Tsai, C –C; Teng, H, Chem. Mater, **2006**, 18, 367
13. Ishikawa, Y.; Matsumoto, Y.; Nishida, Y.; Taniguchi, S.; Watanabe, J. J. Am. Chem. Soc.**, 2003**, 125, 6558.
14. Maeda, K.; Takata, T.; Hara, M.; Saito, N.; Inoue, Y.; Kobayashi, H.; Domen, K. J. Am. Chem. Soc., **2005**, 127, 8286.
15. Yumashev, K. V.; Gurin, V. S.; Prokoshin, P. V.; Prokopenko, V. B.; Alexeenko, A. A. Phys. Stat. Sol., **2001,** 224, 815.

16. Nagesha, D. K.; Liang, X.; Mamedov, A. A.; Gainer, G.; Eastman, M. A.; Giersig, M.; Song, J.-J.; Ni, T.; Kotov, N. A. J. Phys. Chem. B, **2001**, 105, 7490.
17. Beek, W. J. E.; Wienk, M. M.; Kemerink, M.; Yang, X.; Janssen, R. A. J. J. Phys. Chem. B, **2005**, 109, 9505.
18. A. Zaban and et.al J. Phys. Chem. B, **1997**, 101,55-57
19. L. Kavan & Grätzel. Electroch. Acta., **1995**, V 40, No 5.p. 643
20. M. Wei,*Y. Konishi, H. Zhou, M. Yanagida, H. Sugihara* and H. Arakawab J. Mater. Chem., **2006**, 16, 1287–1293